Article

Cite This: *Biomacromolecules* 2019, 20, 2962−2972

pubs.acs.org/Biomac

Glyconanoparticles for Targeted Tumor Therapy of Platinum Anticancer Drug

Aydan Dag,*[,†] Pinar Sinem Omurtag Ozgen,[‡] and Sezen Atasoy[§]

[†]Department of Pharmaceutical Chemistry, Faculty of Pharmacy, and [§]Department of Biochemistry, Faculty of Pharmacy, Bezmialem Vakif University, İstanbul 34093, Turkey

[‡]Department of Analytical Chemistry, School of Pharmacy, Istanbul Medipol University, İstanbul 34810, Turkey

Supporting Information

ABSTRACT: An important requirement to decrease the side effects of chemotherapy drugs is to develop nanocarriers with precise biological functions. In this work, a set of glyconanoparticles was prepared via self-assembly of amphiphilic glycoblock copolymers for the targeted delivery of a hydrophobic chemotherapy drug. Well-defined glycoblock copolymers that consist of 1,1-di-*tert*-butyl 3-(2-(metyloyloxy)ethyl)-butane-1,1,3-tricarboxylate (MAETC) together with three different protected-sugar moieties (*β*-D-glucopyranoside, *β*-D-mannopyranoside, and *β*-L-fucopyranoside) were synthesized by using reversible addition−fragmentation chain-transfer polymerization. Copolymers were deprotected and conjugated with the *cis*-dichlorodiammineplatinum(II) (*cis*-Pt) anticancer drug. Dynamic light scattering and transmission electron microscopy measurements revealed that *cis*-Pt-conjugated glyconanoparticles were sufficiently stable under physiological conditions and had diameters of approximately 100 nm with considerably narrow size distributions. They were intracellularly taken up by the breast cancer (MCF-7 and MDA-MB-231), prostate cancer (PC3), renal cancer (769-P), and Chinese hamster ovary cell lines. The PC3 and 769-P cell lines showed a high preference for the glycosylated nanoparticles. Glycoblock copolymers were found nontoxic but showed high cytotoxicity and increased efficacy after conjugation with the *cis*-Pt anticancer drug. Moreover, in vitro cytotoxicity assays in cancer cell lines demonstrate that *cis*-Pt-loaded glycopolymer-based nanoparticles have higher cytotoxicity than free *cis*-Pt. Overall, our results suggest that glyconanoparticles have a great potential to be used as an effective *cis*-Pt drug carrier for targeted cancer therapy.

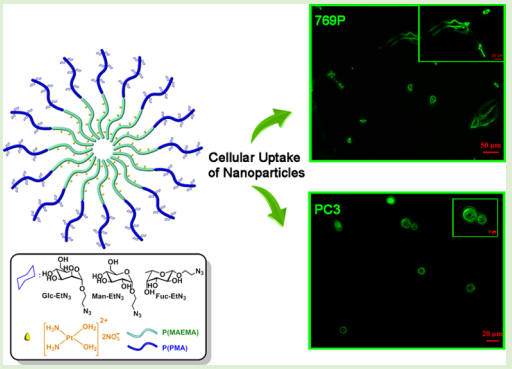

INTRODUCTION

Cancer is still one of the most serious medical problems leading to mortality worldwide. Even though conventional chemotherapeutic agents are still used broadly in cancer therapy, they have some drawbacks such as deficient recognition of tumor tissues that result in damage to healthy tissues as well as low biocompatibility because of their hydrophobicity that leads to aggregation. Therefore, there is an urgent clinical requirement for an effective therapeutic tool to recognize characteristics of healthy cells and cancer cells and simultaneously target cancerous tissue. Smart, sensible, and specific nanocarrier systems for targeted delivery of chemotherapeutic agents are crucial in clinical applications. A range of nanocarrier-based drug delivery systems, comprising polymeric nanoparticles,[1,2] micelles,[3−5] liposomes,[6] and dendrimers,[7−10] have been studied to optimize the therapy regimen for cancer.

Copolymers having both hydrophobic and hydrophilic chains self-assemble into sophisticated nanoparticles with different morphologies (size, shape, composition, structure, etc.) gaining significant interest because of their flexibility in controlling physiological, chemical, and biological properties.[11,12] Core−shell-structured and self-assembled block copolymer nanoparticles have generally been practiced for the drug,[13−15] protein,[16] gene[17] delivery, and imaging agents.[18,19] Most of the synthesized nanoparticles are single-functional; hence, they remain insufficient in a complex physiological environment. This indicates a need to develop innovative multifunctional nanoparticles.[11] Overall, there seems to be essential evidence to indicate that facile, efficient, and stable ligands have critical roles for actively targeting cancer cells.

Performance of an efficient drug release for targeted cancer cells by using nanocarriers can be affected by some parameters such as stimuli-responsive drug release, tumor-targeting ability, cellular internalization, drug loading level, and circulation time. Indeed, numerous studies have attempted to improve the design of the targeted ligands which are directly linked to cancer cellular uptake of nanocarriers to reduce injury in normal tissues.[11] In this respect, nanocarriers derived from the self-assembly of amphiphilic block copolymers provide a broad range of possibilities.[20]

Received: April 17, 2019
Revised: June 21, 2019
Published: July 17, 2019

DOI: 10.1021/acs.biomac.9b00528
Biomacromolecules 2019, 20, 2962−2972

Scheme 1. Schematic Pathway for the Synthesis of *cis*-Pt Conjugated Glyconanoparticles

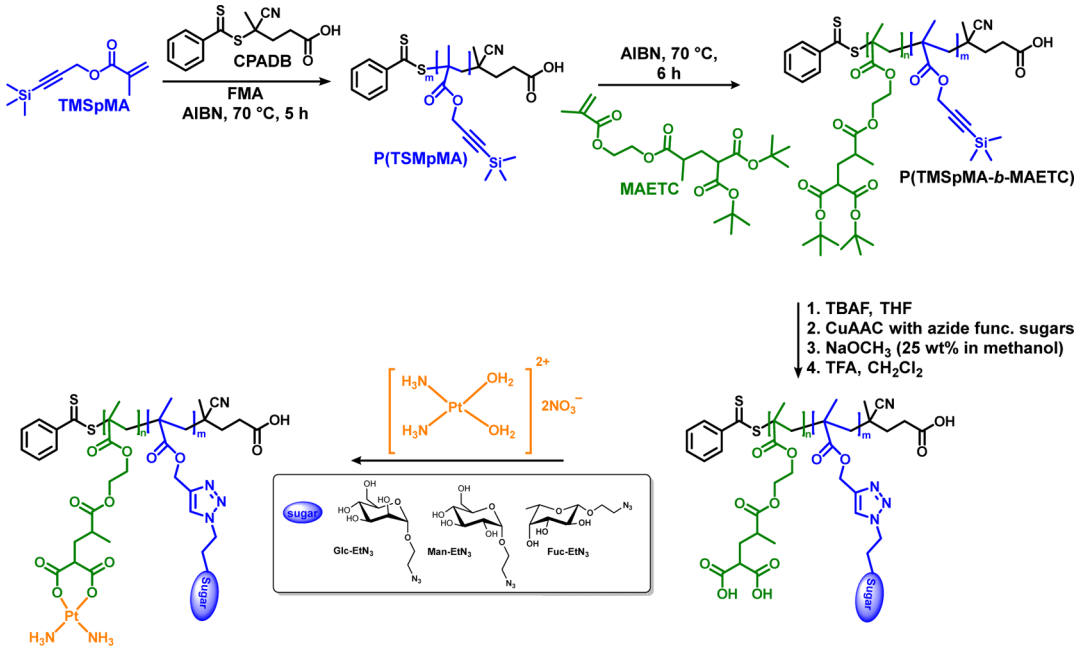

Starting with their synthesis by controlled polymerization techniques, glycopolymers have been known for more than 50 years and enhanced their importance to become a useful tool in drug delivery applications as a result of their recognition properties.[21−23] In addition, glycopolymers have a great potential to increase their specificity by interacting with proteins and cell surfaces in physiological conditions. Interactions between carbohydrates and carbohydrate-binding proteins, such as lectin, are quite weak in biological processes; however, this interaction can be increased by using multimeric carbohydrate molecules which are known as "the cluster glycoside effect".[22,24] Smart glyconanoparticle systems can help to target the drug to tumor side effectively.

Metal-based drugs, especially platinum compounds, have been used as potent anticancer drugs for decades to target against a variety of certain tumors, for example, ovarian, breast, bladder, head, neck, testicular, and lung.[25] Platinum-based drugs such as *cis*-dichlorodiammineplatinum(II) (*cis*-Pt) and carboplatin can be administered alone or in combination with other chemotherapeutic drugs in clinical practice. However, the conventional administration of *cis*-Pt leads to low drug distribution in tumor tissues even though nanocarriers are preferred. Therefore, effective strategies are needed to eliminate side effects and improve the pharmacokinetic properties of *cis*-Pt.[26] Much of the current literature on drug delivery systems pays particular attention to polymeric nanoparticle formulations of *cis*-Pt;[27−29] nonetheless, more practical and nontoxic systems to target tumor tissues selectively and biocompatibly are still in big demand.

More knowledge about oncogenesis revealed that cancer cells have limitless replication potential and deregulate cellular energetics. Higher proliferation index of malignant cells causes increased uptake of glucose for energy production. The regulation of glucose delivery through the cell membrane requires the presence of glucose transporters (GLUT).[30,31] Many members of the GLUT family are described and categorized into three different groups depending on their sequence similarities.[32] It has been well known that GLUT is overexpressed in various types of cancer cells because of the Warburg effect,[33] a deficient mitochondrial oxidative phosphorylation to create adenosine triphosphate (ATP) for energy.[34,35] Under hypoxic conditions, ATP production by cells is dependent on anaerobic glycolysis. However, it has been well known that cancer cells use glycolysis even in the abundance of oxygen. Eventually, glycolysis is enhanced and mitochondrial oxidative phosphorylation capacity is reduced in cancer cells, unlike in healthy cells. The presence of GLUT alterations leads to multiple functional alterations affecting malignant transformation processes and signaling pathways.[36] As it has been demonstrated that the glycolysis pathway is more active in cancer cells,[37,38] GLUTs can be offered as a facilitating candidate for cancer treatment with sugar-decorated nanoparticles.[39−45]

Herein, we synthesized poly(trimethylsilyl-protected propargyl methacrylate-*block*-1,1-di-*tert*-butyl 3-(2-(methacryloyloxy)ethyl)-butane-1,1,3-tricarboxylate) (P(TMSpMA-*b*-MAETC)) diblock copolymers which have side chains consisting of glucose, mannose, and fucose moieties. They were also conjugated with *cis*-Pt through in situ synthesis to produce new glyconanoparticle systems (Scheme 1). Nanoparticles were engineered to entrap *cis*-Pt into glycoblock copolymers providing enhanced colloidal stability, water solubility, and biocompatibility because of the sugar capsule. The resulting glyconanoparticles were confirmed to have a diameter of approximately 100 nm, with narrow size distribution. A safe and efficient nanocarrier system comprising glyconanoparticles for the delivery of chemotherapy drug (*cis*-Pt) was developed and in vitro cell uptaking efficacy in MCF-7, MDA-MB-231, PC3, 769-P, and Chinese hamster ovary (CHO) cell lines were studied. The *cis*-Pt-conjugated glyconanoparticles were tested for cytotoxicity and compared to *cis*-Pt alone, showing that the highest level of cell death appears when *cis*-Pt-loaded glyconanoparticles are simultaneously uptaken and delivered into the cells. As compared to free *cis*-Pt, glyconanoparticles conjugated with *cis*-Pt can

DOI: 10.1021/acs.biomac.9b00528
Biomacromolecules 2019, 20, 2962−2972

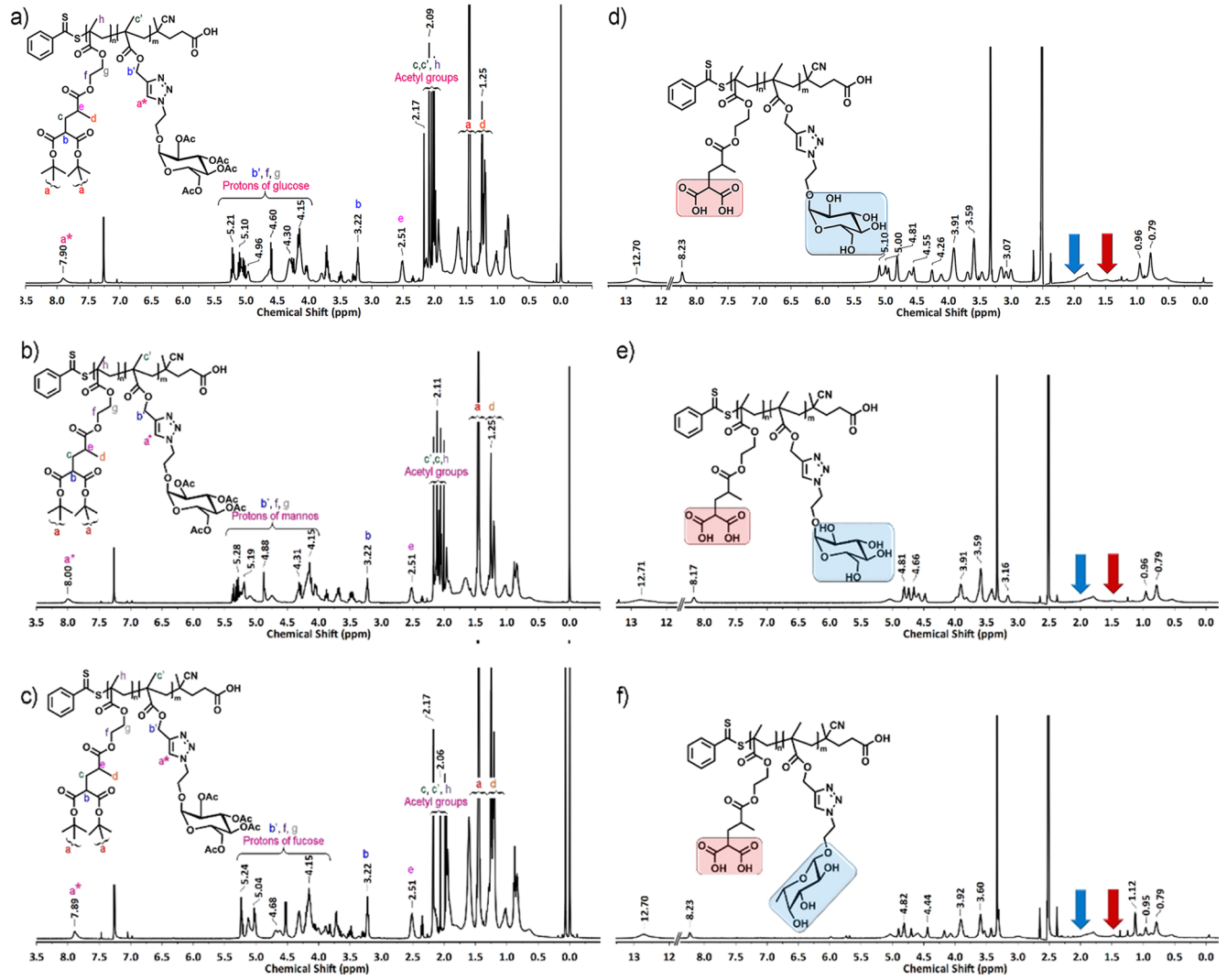

Figure 1. ^{1}H NMR spectra of synthesized (a) P(AcGlcMA-*b*-MAETC), (b) P(AcManMA-*b*-MAETC), (c) P(AcFucMA-*b*-MAETC) (500 MHz, $CDCl_3$) and (d) P(GlcMA-*b*-MAEMA), (e) P(ManMA-*b*-MAEMA), and (f) P(FucMA-*b*-MAEMA) glycoblock copolymers (500 MHz, DMSO-d_6).

selectively induce apoptosis of cancer cells upon altering sugar units.

EXPERIMENTAL PROCEDURES

Materials and Methods. D-Glucose, D-mannose (Sigma, ≥99%), L-fucose, and fluorescein *O*-methacrylate (FMA, Aldrich, 95%) were used as received. *N*,*N*,*N*′,*N*″,*N*″-Pentamethyldiethylenetriamine (PMDETA, Sigma-Aldrich, 99%) was passed through a basic alumina column to remove the inhibitor. Copper(I) bromide (CuBr, Sigma-Aldrich, 99.9%), tetrahydrofuran anhydrous (THF, Sigma-Aldrich), sodium azide (NaN_3, Acros, 99%), trifluoroacetic acid (TFA, Acros, 99%), dimethyl sulfoxide (DMSO, Merck, 98.9%), petroleum spirit (BR 40−60 °C, Merck, 90%), diethyl ether (Merck, 99%), THF (Merck, 99.7%), dichloromethane (CH_2Cl_2, anhydrous, >99.8%, Aldrich), and 1,4-dioxane (Merck, 99%) were used without further purification. Sulfuric acid (95−98%, Merck) was used as received. 2,2′-Azobis(isobutyronitrile) (AIBN, Fluka, 98%) was recrystallized from methanol. Unless otherwise specified, all chemicals were of reagent grade and used as received. Ultrapure (UP) water was produced by a Milli-Q reverse osmosis system and had a resistivity of 19.6 MΩ·cm. Dulbecco's modified Eagle medium/nutrient mixture F-12 (DMEM/F12) medium, fetal bovine serum (FBS), 0.25% trypsin/0.20% ethylene diamine tetraacetic acid (EDTA), phosphate-buffered saline (PBS), penicillin/streptomycin, and L-glutamine were purchased from Thermo Fisher Scientific. MTT assay kit was purchased from Sigma-Aldrich. T flasks, 96-well plates, and cell culture supplies were purchased from Corning Inc. (Corning, NY).

Synthesis of Reversible Addition−Fragmentation Chain-Transfer Agent, Monomers, and Azido-Functionalized Sugar Moieties. 2-Azidoethyl 2,3,4,6-tetra-*O*-acetyl-*β*-D-glucopyranoside (AcGlc-EtN_3), 2-azidoethyl 2,3,4,6-tetra-*O*-acetyl-*β*-D-mannopyranoside (AcMan-EtN_3), and 2-azidoethyl 2,3,4-tri-*O*-acetyl-*β*-L-fucopyranoside (AcFuc-EtN_3) were synthesized according to the published procedure.[3,46] The synthesis of 4-cyanopentanoic acid dithiobenzoate (CPADB) was described in the literature.[47] 3-(Trimethylsilyl)prop-2-yn-1-ylmethacrylate (TMSpMA)[3] and 1,1-di-*tert*-butyl 3-(2-(methacryloyloxy)ethyl)-butane-1,1,3-tricarboxylate (MAETC)[13] were prepared according to published procedures.

Preparation of P(TMSpMA). P(TMSpMA) was prepared via reversible addition−fragmentation chain-transfer (RAFT) polymerization method according to a modified procedure.[3] CPADB RAFT agent (0.057 g, 0.204 mmol), 3-(trimethylsilyl)prop-2-yn-1-ylmethacrylate (TMSpMA) (2.00 g, 10.20 mmol), AIBN (4.187 mg, 0.025 mmol), and FMA (0.040 g, 0.102 mmol) for fluorescent labeling were added into a septa-sealed round-bottom flask and dissolved in toluene (5 mL). The polymerization flask was placed in an ice bath, and the reaction solution was deoxygenized with a continuous flow of

DOI: 10.1021/acs.biomac.9b00528
Biomacromolecules 2019, 20, 2962−2972

nitrogen for 60 min. The ratio between the monomer, RAFT agent, and AIBN ($[monomer]_0/[RAFT]_0/[initiator]_0$) in the polymerization medium was 50:1.0:0.125. After purging, the reaction mixture was then put into a silicone oil bath at 70 °C. The homopolymerization reaction was quenched after 5 h via rapid cooling and exposure to oxygen. The ^{1}H NMR (nuclear magnetic resonance) sample of polymerization was taken to determine the monomer conversion. The conversion was calculated from the relative integration of monomer's vinylic peaks ($CH{=}{=}CH_2$, 6.17−5.61 ppm) and the polymer's $-OCH_2$ peak at 4.76−4.56 ppm. The polymerization solution was concentrated by partial evaporation of toluene, and then the polymer was precipitated in 10-fold excess of cold methanol two times to remove the unreacted monomers (TMSpMA and FMA) and the RAFT agent. Then, the purified polymer was dried under vacuum overnight to give 1.30 g of a pink solid. On the basis of TMSpMA conversion of 70%, the yield of the polymer was calculated as 65%. The purified polymer was further characterized by ^{1}H NMR and gel permeation chromatography (GPC) measurements (details are given in the Supporting Information, Figures S12 and S15).

^{1}H NMR ($CDCl_3$, 500 MHz): 7.86−7.23 (5H, aromatic protons), 4.76−4.56 (br, 2H, $-OCH_2$), 2.43 (4H, $-CH_2CH_2COOH$), 2.18 (br, 3H, CH_3COO-), 0.20−0.09 (br, 9H, $Si(CH_3)_3$).

Preparation of P(TMSpMA-*b*-MAETC). The previously obtained P(TMSpMA), which was used as a macro-RAFT agent (0.972 g, 0.136 mmol, $M_{n,NMR}$ = 7150 g/mol), MAETC (5.64 g, 13.61 mmol), AIBN (4.47 mg, 0.027 mmol), and 6 mL of toluene were added in a septa-sealed round-bottom flask. After purging with nitrogen for an hour, the flask was transferred into a silicone oil bath at 70 °C for 6 h. The diblock copolymer was purified by precipitation twice in methanol. Then, it was dried under vacuum overnight at 25 °C to give 3.61 g of a pale pink solid. On the basis of P(TMSpMA-*b*-MAETC) conversion of 77%, the yield of the polymer was calculated as 68%. The purified polymer was characterized by ^{1}H NMR and GPC measurements (details are given in the Supporting Information, Figures S13 and S15).

^{1}H NMR ($CDCl_3$, 500 MHz): 7.86−7.23 (5H, aromatic protons), 4.76−4.56 (2mH, $-COOCH_2CCSi$), 4.14 (4nH, $-OCH_2CH_2O-$), 3.22 (1H, $OOCCHCH_3CH_2CH(COOBu\text{-}tert)_2$), 2.50 (br, 1H, $OOCCHCH_3CH_2CH(COOBu\text{-}tert)_2$), 2.17−2.10 (2nH + 3nH + 3mH, CH_3 attached to the backbone of MAETC and TMSpMA, 2H, $OOCCHCH_3CH_2CH(COOBu\text{-}tert)_2$), 1.47−1.43 (18nH, $OOCCHCH_3CH_2CH(COO(CH_3)_3)_2$), 1.3−1.1 (3nH, $OOCCHCH_3CH_2CH(COOBu\text{-}tert)_2$), 1.06−0.86 (2nH + 2mH, CH_2 of the main chain of TMSpMA and MAETC, respectively), 0.20−0.09 (br, 9H, $Si(CH_3)_3$).

Preparation of Poly(propargyl methacrylate-*block*-1,1-di-*tert*-butyl 3-(2-(methacryloyloxy)ethyl)-butane-1,1,3-tricarboxylate) (P(PMA-*b*-MAETC)). The P(TMSpMA-*b*-MAETC) diblock copolymer (0.90 g) was dissolved in THF (25 mL) under nitrogen (ca. 10 min) bubbling and cooled to 0 °C. Then, a solution of TBAF in THF (1 M, 1.5 equiv mol/mol with respect to the trimethylsilyl protected alkyne groups) was added by a dropper via a glass syringe (ca. 2−3 min). The reaction mixture was stirred at 0 °C for 30 min and then warmed to ambient temperature. The deprotection reaction was complete within 2 h. The solution was evaporated and dialyzed against first UP water/THF solution (1/1, v/v) and then THF for 2 days. The solution was evaporated and dried in a vacuum oven at room temperature for 24 h. The disappearance of trimethylsilyl groups was verified by ^{1}H NMR with the absence of signals at 0.20 ppm (details are given in the Supporting Information, Figure S14).

General Procedure for Preparation of Glycoblock Copolymer via Azide−Alkyne Click Reaction. P(PMA-*b*-MAETC) (0.200 g, 5.479 μmol, $M_{n,NMR}$ = 36 500 g/mol, 1 equiv), 2-azidoethyl 2,3,4,6-tetra-*O*-acetyl-β-D-glucopyranoside (AcGlc-EtN_3) (0.230 mmol, 1.2 equiv for every alkyne unit), PMDETA (0.080 mL, 0.383 mmol, 2 equiv for every alkyne unit), CuBr (0.055 g, 0.383 mmol, 2 equiv for every alkyne unit), and dimethylformamide (DMF, 2 mL) were added to a 16 mL Schlenk tube. The reaction mixture was degassed by three freeze−pump−thaw cycles, left under vacuum, and stirred overnight at 35 °C.

Subsequently, the solution was filtered through a column filled with neutral alumina to remove the copper complex and purified by dialysis against UP water [molecular weight cutoff (MWCO) 1000 Da] for 4 days and collected by lyophilization. The purified polymer was characterized by ^{1}H NMR and GPC measurements (Figure S16). The same procedure has been followed to obtain two more different glycoblock copolymers by using AcMan-EtN_3 and AcFuc-EtN_3 separately. Representative ^{1}H NMR (500 MHz, $CDCl_3$) spectra and signal assignments for all glycopolymers are presented in Figure 1a−c.

General Procedure for Deprotection of Glycoblock Copolymers (P(GlcMA-*b*-MAEMA), P(ManMA-*b*-MAEMA), and P(FucMA-*b*-MAEMA)). The acetyl groups of sugar units were deprotected in terms of basic treatments of the glycoblock copolymer scaffold. In a general procedure, P(AcGlcMA-*b*-MAETC) (0.100 g, 1.998 μmol, $M_{n,NMR}$ = 50 050 g/mol) was dissolved in a $CHCl_3$/CH_3OH mixture (25 mL, 1/1, v/v). The reaction solution was bubbled with nitrogen flow for 30 min. The freshly prepared $NaOCH_3$ (25 wt % in methanol) in a dry solution of methanol (0.092 M) was introduced into the reaction mixture by dropping the appropriate quantity (0.015 mL, 0.25 equiv per acetyl group, and 0.065 mmol) via a syringe. The reaction mixture was stirred for 3 h at room temperature. After that, the solvent was removed under vacuum at ambient temperature. The residual 2 mL polymer solution was subsequently dialyzed against UP water for 2 days (MWCO 3500 Da). The deprotected glycoblock copolymers (P(GlcMA-*b*-MAETC), P(ManMA-*b*-MAETC), and P(FucMA-*b*-MAETC)) were recovered by lyophilization.

After that, the *tert*-butoxy group deprotection of the glycoblock copolymers were carried out under acidic conditions. As a general procedure, the glycoblock copolymer (60 mg) and TFA/H_2O (4 mL, 9:1, v/v) were put into a 25 mL round-bottom flask. The turbid reaction solution became clear during stirring at room temperature. After 2 h of reaction, the polymer solution was dialyzed against UP water for 2 days (MWCO 3500 Da). Deprotected polymers were collected after lyophilization as a fluffy solid. The purified polymer was characterized by ^{1}H NMR, Fourier transform infrared (FT-IR), and GPC measurements (Figures S17 and S18). Representative ^{1}H NMR (500 MHz, DMSO-d_6) spectra and signal assignments for all glycopolymers are presented as P(GlcMA-*b*-MAEMA), P(ManMA-*b*-MAEMA), and P(FucMA-*b*-MAEMA) as shown in Figure 1d−f.

Preparation and Characterization of *cis*-Pt-Loaded Glyconanoparticles. The synthesis procedure of *cis*-Pt was adapted from the literature.[48] Glycoblock copolymer (10 mg, 25.61 μmol) dissolved in DMF (1 mL) was mixed with NaOH (1 M) (6 mg, 0.15 mmol). The mixture was stirred for 30 min at room temperature, and then the *cis*-Pt solution in UP water was added via a syringe pump at 0.5 equivalent concentration (0.5 equiv per carboxylic acid group of P(MAEMA)) to react for 24 h at room temperature and stirred in a dark environment. To increase the drug loading efficiency, the micelle solutions were further stirred in an orbital shaker for 2 days at 37 °C.

The *cis*-Pt glycoblock copolymer conjugate was subsequently dialyzed against UP water (MWCO 3500 Da). Upon changing the dialysate to UP water, the *cis*-Pt-conjugated glycopolymer self-assembled into nanoparticular drug carriers. Next, the nanoparticular solution was further purified by using 0.22 μm syringe filters.

Throughout this paper, the term NP1 will refer to P(GlcMA-*b*-MAEMA)/Pt, the term NP2 will refer to P(ManMA-*b*-MAEMA)/Pt, and the term NP3 will refer to P(FucMA-*b*-MAEMA)/Pt.

In Vitro Drug Release of *cis*-Pt. The release rate of *cis*-Pt from NP3 was evaluated by the dialysis method in two different pH buffer solutions (pH = 5.5 and pH 7.4). In brief, *cis*-Pt-loaded glyconanoparticles were placed into a dialysis cell with a MWCO of 3500 Da. Glyconanoparticles were dialyzed against 80 mL of PBS containing (10 mM) 150 mM NaCl at slightly alkaline and endosomal pH (pH 5.5) in physiological conditions in a thermo-controlled shaker with a stirring speed of 120 rpm at 37 °C. The samples were digested in concentrated nitric acid/hydrochloric acid solutions (v/v, 3/1) at 80 °C for 1 h. The concentration of Pt was obtained by using

DOI: 10.1021/acs.biomac.9b00528
Biomacromolecules 2019, 20, 2962−2972

Table 1. Molecular Characteristics and Composition of Glycoblock Copolymers and Their Precursors

entry	polymer	conv.[d] (%)	$M_{n,NMR}$[e]	$M_{n,GPC}$[f]	$Đ$
1	P(TMSpMA)[a]	70	7150	9700	1.17
2	P($TMSpMA_{35}$-*b*-$MAETC_{77}$)[b]	77	39 000	32 300	1.26
3	P(PMA_{35}-*b*-$MAETC_{77}$)[c]	>99	36 500	42 800	1.27
4	P(AcGlcMA-*b*-MAETC)	>98	50 050	50 400	1.36
5	P(AcManMA-*b*-MAETC)	>98	50 050	52 560	1.36
6	P(AcFucMA-*b*-MAETC)	>98	49 100	48 750	1.41
7	P(GlcMA-*b*-MAEMA)	>95	38 150	40 180[g]	1.18
8	P(ManMA-*b*-MAEMA)	>95	38 150	40 150[g]	1.18
9	P(FucMA-*b*-MAEMA)	>95	35 800	37 200[g]	1.17

[a][M]/[FMA]/[RAFT]/[I] = 50:0.5:1:0.125 polymerization was carried out at 70 °C for 5 h. [b][M]/[macro-RAFT]/[I] = 100:1:0.2 polymerization was carried out at 70 °C for 6 h. [c]After hydrolysis reaction. [d]Determined by ^{1}H NMR. [e]$M_{n,NMR}$ = DP_n determined from ^{1}H NMR × M_W of monomer + M_W of RAFT agent. [f]Determined by conventional THF-GPC (RI detection) relative to linear PS standards. [g]Determined by DMF-GPC (MALS/RI/UV/dQLS detection) as M_w values.

inductively coupled plasma mass spectrometry (ICP-MS, Agilent 7700 ICP-MS). The 1 mL of samples were taken from the dialysis medium at a certain time point for ICP-MS measurement and were replaced in the same volume of the fresh media. The quantity of drug released into the media at each time interval was calculated as the percentage of total drug released to the initial amount of the drug.[13] It is shown in Figure S22.

Turbidimetric Assay. The lectin recognition binding activity of the P(ManMA-*b*-MAEMA) and P(ManMA-*b*-MAEMA)/Pt (NP2) solutions was analyzed using a turbidimetric assay via UV−vis spectroscopy (Hitachi U-2900). The experimental procedure is detailed in the Supporting Information.[49] The turbidimetric assay measurements are shown in Figure S23.

In Vitro Cell Culture and Cytotoxicity Assay. Human breast cancer (MCF-7 and MDA-MB-231), prostate cancer (PC3), renal cancer (769-P), and CHO cell lines were purchased from the American Tissue Culture Collection. The cells were cultured in a T25 cell culture flask with a humid environment in a 5% CO_2 atmosphere at 37 °C in DMEM/F12 supplemented with 10% FBS and 100 U/mL of penicillin/streptomycin. After the cells reached convenient confluency (80%), the cells were washed with PBS and detached by trypsin/EDTA treatment. Finally, the cells were collected, centrifuged, and resuspended in the culture medium for further experiments.

The cytotoxicities of NP1, NP2, NP3, P(GlcMA-*b*-MAEMA), P(ManMA-*b*-MAEMA), P(FucMA-*b*-MAEMA), and free *cis*-Pt were evaluated on MCF-7, MDA-MB-231, PC3, 769-P, and CHO cell lines by the standard MTT (3-(4,5-dimethylthiazol-2-yl)-2,5-diphenyltetrazolium bromide) assay according to the procedure given in the Supporting Information.

Cellular Uptake of Glyconanoparticles. Cellular uptake was evaluated through measurement of the intracellular fluorescence following incubation with the fluorescein-labeled glyconanoparticles. Briefly, cells were seeded in a 35 mm FluoroDish (World Precision Instruments) at a density of 2 × 10^5 per dish in 3 mL of growth medium and cultured for 1 day with DMEM/F12 cell culture medium. The glyconanoparticle solution was loaded onto the cells at a working concentration of 100 μg/mL and incubated at 37 °C for 2 h. After incubation, the cells were washed three times with PBS and then uptake of glyconanoparticles was observed under a fluorescence microscope system (Zeiss Axio Observer Z1, excitation wavelengths: 405 nm, 488, and 561 nm, 20×/1.4 NA objective lens). The ZEN2 imaging software (Zeiss) was used for image acquisition and processing.

Fifteen images of cellular internalized NPs were captured using the same exposure time of 500 ms, and total fluorescence intensity of randomly selected 10 cells were determined using ImageJ software.[50] Briefly, cells of interest were selected for each image and fluorescence intensity was measured. The regions out of the cells were classified as background. Corrected total cell fluorescence (CTCF) was then obtained by subtracting the background from the integrated density (IntDen). CTCF and IntDen values for a selected cell of interest between all cell lines are shown in Figure S25. Statistical analyses were performed by Graphpad Prism 8.00. Cellular internalization efficiency was also quantified by a flow cytometry BD Accuri C6 (BD Biosciences, San Jose, USA) and is explained in the Supporting Information.

Apoptosis Assays. The cell lines were treated with the different *cis*-Pt-loaded glyconanoparticles and supplemented with nutrient medium. After incubating for 24 h, the cells were detached from their culture vessel. Fresh serum/phenol red-free, 1% bovine serum albumin (10 μg/mL) containing medium was added to each sample. Analysis of live, early, late apoptosis, and cell death was carried out using the Muse Annexin V and Dead Cell Assay kit (Muse Cell Analyzer, Millipore Corp.) according to the manufacturer's instructions.[51]

RESULTS AND DISCUSSION

Syntheses of Glycoblock Copolymers. The P(TMSpMA-*b*-MAETC) diblock copolymer was obtained in two steps using the strategy previously described by Babiuch et al.[3] First, P(TMSpMA-*b*-MAETC) was synthesized via a sequential RAFT polymerization method of TMSpMA monomer, followed by MAETC to grow the second block (Figures S12 and S13). In the synthesis of first block, FMA also was added into the mixture as a fluorescein dye to tag glyconanoparticles for evaluating in vitro cellular uptake studies. The $M_{n,GPC}$ value of the homopolymer (P(TMSpMA)) was obtained as 9700 g/mol with 1.17 polydispersity. The GPC chromatogram as shown in Figure S15 confirmed the successful synthesis of P(TMSpMA-*b*-MAETC) with a number-average molecular weight of 32 300 g/mol and a relatively low polydispersity (Table 1). After polymer purification, the trimethylsilyl groups of the block copolymer were deprotected in the presence of TBAF and purified by the dialysis method to give alkynyl side groups of P(PMA-*b*-MAETC). According to the ^{1}H NMR analysis, the successful deprotection of the trimethyl silyl group into an alkynyl group was confirmed by the disappearance of the trimethylsilyl signal at 0.20 ppm and the appearance of a new signal regarding the alkynyl side groups at 2.27 ppm (Figure S14). Additionally, GPC analysis revealed a slight increase of M_n with a similar polydispersity index after deprotection of the trimethylsilyl group regarded as a change of hydrodynamic volume while showing no degradation of the polymer (Figure S15).

Subsequently, the functionalization of the alkynyl side groups of the diblock polymer (P(PMA-*b*-MAETC)) was performed via the copper-catalyzed azide−alkyne cycloaddition reaction of azido-functionalized sugar moieties

DOI: 10.1021/acs.biomac.9b00528
Biomacromolecules 2019, 20, 2962−2972

Table 2. Characterization of *cis*-Pt-Conjugated Glyconanoparticles

code	polymer	*cis*-Pt feeding [*cis*-Pt]/[COOH]	conjugation ratio [*cis*-Pt]/[COOH][a]	D_h (nm)[b]	$Đ$[b]	ζpot (mV)[b]
NP1	P(GlcMA-*b*-MAEMA)/Pt	0.5	57[a]	106 ± 5	0.182	−14.2 ± 1.7
NP2	P(ManMA-*b*-MAEMA)/Pt	0.5	46[a]	97 ± 3	0.087	−17.1 ± 0.7
NP3	P(FucMA-*b*-MAEMA)/Pt	0.5	45[a]	97 ± 2	0.117	−20.8 ± 0.9

[a]Determined by ICP-MS. [b]Number distribution determined by DLS.

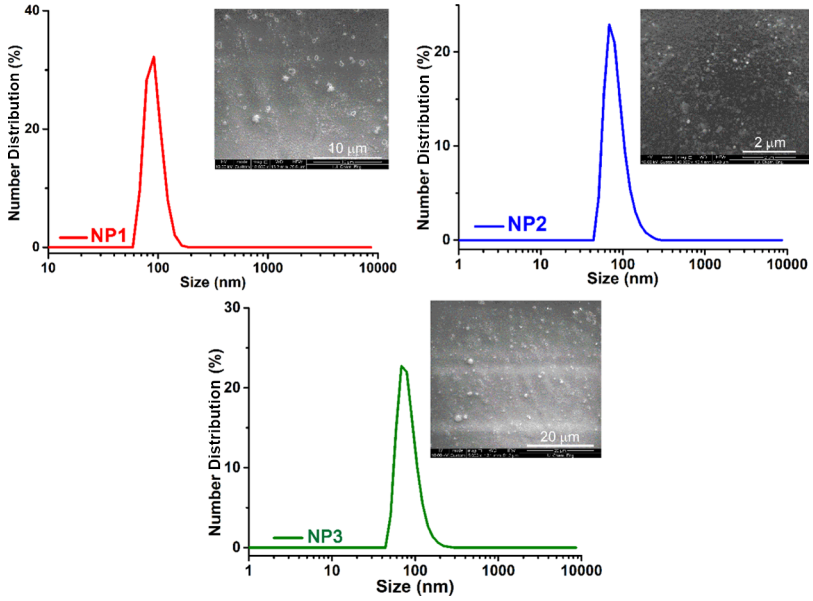

Figure 2. SEM images (inset) and DLS graphs of NP1, NP2, and NP3. All samples were measured at the concentration of 1 mg/mL for DLS analysis.

composed of acetyl protected-sugar moieties 2-azidoethyl 2,3,4,6-tetra-*O*-acetyl-*β*-D-glucopyranoside (AcGlc-EtN_3), 2-azidoethyl 2,3,4,6-tetra-*O*-acetyl-*β*-D-mannopyranoside (AcMan-EtN_3), and 2-azidoethyl 2,3,4-tri-*O*-acetyl-*β*-L-fucopyranoside (AcFuc-EtN_3) in DMF with a CuBr/PMDETA catalyst. The copper catalyst was removed by passing it through a short column of neutral alumina and then dialyzed against UP water (see the Experimental Proceduressection) for 4 days. Glycoblock copolymers were obtained as white powders. The ratio of sugar moieties grafted to P(PMA-*b*-MAETC) was calculated by comparing the integrated peak areas from the ^{1}H NMR spectrum of the triazole peak (7.90−8.00 ppm) to that of the COC*H*CH_3 peak (2.51 ppm) of MAETC repeating unit. According to Figure 1a−c, the click efficiency was found higher than 98%.

This approach created a small library of three different glycoblock copolymers that have the same backbone (Figure 1a−c). Table 1 summarizes the molecular weight data of both homopolymer and glycoblock copolymers elaborated from GPC measurements.

Aqueous basic treatment of P(AcGlcMA-*b*-MAETC), P(AcManMA-*b*-MAETC), and P(AcFucMA-*b*-MAETC) glycoblock copolymers to remove the acetyl groups of sugar units gave the desired P(GlcMA-*b*-MAEMA), P(ManMA-*b*-MAEMA), and P(AcFucMA-*b*-MAEMA) copolymers good yields and purities. The resulting glycoblock copolymers and their precursors were characterized by ^{1}H NMR. Monomodal GPC traces and narrow molecular weight distributions for glycoblock copolymers were detected. Because the ester groups present in the MAETC units (i.e., *tert*-butyl ester) have different stability, it was possible to selectively deprotect the *tert*-butyl ester groups by treatment with a mixture of CH_2Cl_2 and TFA, affording to acid groups in predetermined positions. The ^{1}H NMR spectra of P(GlcMA-*b*-MAEMA), P(ManMA-*b*-MAEMA), and P(FucMA-*b*-MAEMA) in DMSO-d_6 showing quantitative removal of the acetyl (no signal at ∼2.09 ppm) and *tert*-butyl groups (no *tert*-butyl signal at 1.41 ppm) (Figure 1d−f). The GPC traces of resulting deprotected glycoblock copolymers showed monomodal distribution (Figure S18). Moreover, all diblock glycopolymers were obtained with an M_w of between 40 180 and 37 200 and polydispersity at around 1.18 (Table 1, entries between 7 and 9, Figure S18).

Moreover, fluorescence spectroscopy measurements of the FMA-tagged resulting polymers (P(GlcMA-*b*-MAEMA), P(ManMA-*b*-MAEMA), and P(FucMA-*b*-MAEMA)) show spectra comparable to that of each other with small differences in fluorescence intensity because all three glycoblock copolymers have the same backbone (Figure S20).

In Situ Drug Loading and Self-Assembly of Glycoblock Copolymers. *cis*-Pt-loaded glyconanoparticles were synthesized according to the previously reported procedure.[52] It has been observed that three glycoblock copolymers presented in Table 1 (entries between 7 and 9) have good solubility in water. Diblock glycopolymers were conjugated with *cis*-Pt and subsequently self-assemble to form nanosized structures in aqueous solutions with a *cis*-Pt core surrounded by a glycopolymer shell. The hydrodynamic sizes, size distributions, and surface charges of the assemblies formed in aqueous solutions from the *cis*-Pt-loaded glycoblock copolymers NP1, NP2, and NP3 were evaluated by dynamic light scattering (DLS) measurements and the morphology of the assemblies was evaluated by scanning electron microscopy

DOI: 10.1021/acs.biomac.9b00528
Biomacromolecules 2019, 20, 2962−2972

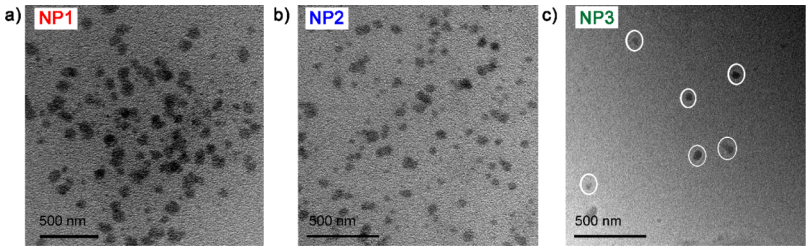

Figure 3. TEM images of (a) NP1, (b) NP2, and (c) NP3 (scale bar is 500 nm).

Table 3. Comparison of IC_{50} Values for *cis*-Pt and *cis*-Pt-Loaded Glyconanoparticles, $n = 3$[a]

	IC_{50} value (μM)			
cell lines	*cis*-Pt	NP1	NP2	NP3
MCF-7	5.16 ± 0.11	9.93 ± 0.10	14.12 ± 0.12	12.73 ± 0.06
MDA-MB-231	3.27 ± 0.15	8.02 ± 0.13	7.62 ± 0.06	9.42 ± 0.17
PC3	2.18 ± 0.02	0.51 ± 0.23	1.23 ± 0.07	1.93 ± 0.27
769-P	2.08 ± 0.94	0.46 ± 1.04	1.32 ± 0.22	1.61 ± 0.18
CHO	18.66 ± 1.85	16.11 ± 0.46	17.10 ± 0.26	16.00 ± 1.13

[a]Data were presented as mean ± standard deviation.

(SEM) and transmission electron microscopy (TEM) (Table 2).

The hydrodynamic sizes of the glycoblock copolymers in aqueous solution before the treatment with *cis*-Pt were also determined by DLS with a condition similar to that of glyconanoparticles (Figure S19). DLS measurements of glycoblock copolymers showed that the hydrodynamic diameter of the NPs increased after the *cis*-Pt conjugation. Additionally, DLS results demonstrated unimodal distributions with number-average hydrodynamic diameters (D_h) ranging between 97 and 106 nm in UP water (Figure 2). The surface charges of the nanoparticles were assessed by means of their zeta potentials (ζpot), as determined by light scattering, which were negative in all cases with values in the −14 to −20 mV range. *cis*-Pt-loaded NPs remained well dispersed and colloidally stable, without size difference during the following week.

SEM and TEM images were conducted to characterize the size of the NPs. As shown in Figure 2, the SEM images show spherical sizes of NPs. The TEM images displayed that NPs were well distributed without apparent particle aggregation, and the average diameter was less than 100 nm around. The TEM demonstrates slightly smaller sizes, whose size discrepancy was probably due to the dehydration of the glyconanoparticles (Figure 3).

cis-Pt loading capacity was measured by thermogravimetric analyses (TGA) and ICP-MS. A significant amount of glyconanoparticle solutions were lyophilized, weighed, and analyzed by TGA and the loading of Pt in the glyconanoparticles was calculated as 18.04, 13.88, and 14.15% for NP1, NP2, and NP3, respectively (weight of drug/weight of polymer: w/w %, Figure S21). Moreover, the Pt content of a significant amount of glyconanoparticle solutions was quantified by ICP-MS. The Pt concentration of glyconanoparticles was determined to be 19.77, 14.96, and 15.27% for NP1, NP2, and NP3, respectively. The conjugation efficiencies were measured to be 57, 46, and 45% based on the dicarboxylic groups of NP1, NP2, and NP3, respectively (Table 2). Steric hindrance of polymer-limited full platinum conjugation.[13,53]

pH-Triggered *cis*-Pt Release from Glyconanoparticles. *cis*-Pt-loaded glyconanoparticles showed high stability in UP water over an extended period. On the other hand, the presence of sodium chloride in a physiological medium leads to the release of *cis*-Pt gradually. *cis*-Pt released from NP3 was measured by ICP-MS. The release rate profiles of *cis*-Pt from NP3 were investigated in a dialyzing tube resembling physiological conditions in PBS at 37 °C at different pH values (pH 5.5 and pH 7.4). The release of the *cis*-Pt from glyconanoparticular solutions was observed over 4 days. After the treatment of concentrated acid (HNO_3/HCl) at 80 °C for 1 h, the samples were diluted with UP water and analyzed by ICP-MS (Figure S22). No initial burst release was revealed in glyconanoparticle solutions and the release reached a plateau at around 90 and 60% at pH 5.5 and pH 7.4, respectively. The rate of Pt-drug release at pH 5.5 is expectedly higher than pH 7.4, and the plateau at pH 7.4 following the *cis*-Pt release can be related with the resulting polymeric glyconanoparticle structures, which has a high content of negative charges because of the existence of carboxylic groups.[53,54]

In order to evaluate the bioactivity of P(ManMA-*b*-MAEMA) glycopolymer solution and its *cis*-Pt conjugate, turbidimetric assay was conducted. As can be seen from Figure S23, the biological activity of the glycopolymer solution and the glyconanoparticle solution were qualitatively confirmed with the formation of a cluster resulting from the interaction with ConA.

In Vitro Cytotoxicity of Glyconanoparticles and Their Cellular Uptake. The toxicities of NP1, NP2, NP3, glycoblock copolymers, and free *cis*-Pt were assessed against MCF-7, MDA-MB-231, PC3, 769-P, and CHO cell lines. The half maximal inhibitory concentration (IC_{50}) of the NP1, NP2, NP3, and glycoblock copolymers is determined in Figure S24 and is summed up in Table 3. First, glycoblock copolymers were found to be nontoxic at all concentrations (up to 280 μM) after 48 h. Hence, any further effect from *cis*-Pt-loaded glyconanoparticles on cell viability cannot be attributed to the toxicity of polymers. CHO was less affected than MCF-7, MDA-MB-231, PC3, and 769-P to both free and conjugated *cis*-Pt. The IC_{50} values of NP1, NP2, and NP3 for the MCF-7, MDA-MB-231, PC3, and 769-P were ∼3 times higher than those for CHO. It is apparent from Table 3 that NP1, NP2, and NP3 present enhanced toxicity (lower values in IC_{50}) than

DOI: 10.1021/acs.biomac.9b00528
Biomacromolecules 2019, 20, 2962−2972

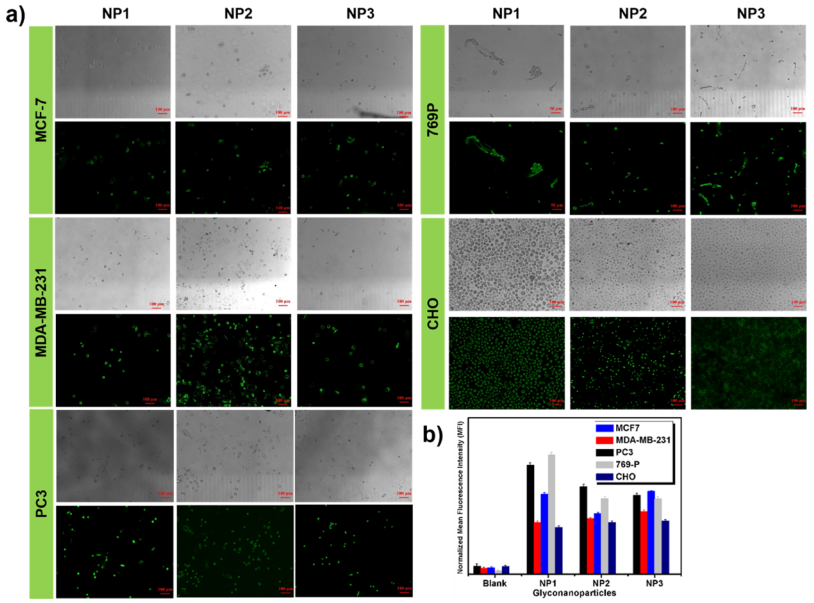

Figure 4. (a) Fluorescence microscopy images with 50 and 100 μm scale and (b) quantitative analysis graph by flow cytometry for the cell uptake upon incubating cells with NP1, NP2, and NP3 at 37 °C for 4 h with cells untreated as a control.

cis-Pt alone toward PC3 and 769-P, compared to other cell lines (Figure S24). *cis*-Pt-loaded glyconanoparticles were revealed higher activity than free *cis*-Pt presumably because of different cellular uptake mechanisms of the glyconanoparticles. An additional reason for the increased cytotoxicity of these glyconanoparticles can be explained by transporter-mediated uptake.

For further analysis of the biological activities and intracellular localization of glyconanoparticles, all cell lines were studied using fluorescence microscopy. Cells were incubated with glyconanoparticles (100 μM) at 37 °C for 2 h. As shown in Figure 4a, FMA-tagged glyconanoparticles were observed in cell sections for all NPs. More fluorescence expression indicated more accumulation induced by various *cis*-Pt formulations. CTCF values were found statistically significant using one-way analysis of variance ($p < 0.0323$) (Figure S25). Besides, uptake of NP1 and NP2 was apparently higher than that of NP3 for PC3 and 769-P cell lines. On the other hand, NP1, NP2, and NP3 exhibited similar internalization properties in MCF-7 and MDA-MB-231 cancer cells (Figure S25). Similarly, flow cytometry analysis also showed that the cellular uptake property of glyconanoparticles was higher based on the fluorescence intensity after administering for 4 h. NP1 exhibited significantly enhanced cellular accumulation than NP2 and NP3 for PC3 and 769-P cancer cells. Flow cytometry results (Figure 4b) were also consistent with the results of fluorescence microscopy.

In the light of obtained results, it is possible to hypothesize that GLUT transporters which showed elevated expression in renal and prostate cancer[55] could cause raised ability for cellular internalization of NPs. Therefore, these results provide the potential application of glyconanoparticles as efficient drug delivery systems for prostate and renal cancers.

It is slightly surprising that lower cytotoxicity and uptake of NPs in breast cancer cell lines were noted in the study (Table 3 and Figure 4b) as numerous studies have shown that GLUTs are expressed in breast cancer cell lines.[56−58] The possible explanations for these results may be that the sugar-decorated nanoparticle concentrations are lower for toxicity and cell metabolism causes growth advantages potentially because of the intracellular effector pathways participating in the stimulation of GLUTs.

Cell Apoptosis. In order to identify the effect of actively internalized NPs, Muse Annexin V/Dead Cell kit (Merck-Millipore, Darmstadt, Germany) staining was performed. The apoptotic index of NP1, NP2, NP3, and free *cis*-Pt treatment was evaluated. An average of at least 5×10^4 cells was analyzed. The representative apoptosis results are shown in Figure S26 and the summary of data are given in Table 4. These results confirm that *cis*-Pt was unable to induce high levels of apoptosis (in particular, compare panels shown in Figure S26). The different degrees of apoptosis appeared in the *cis*-Pt and NPs. Cells treated with *cis*-Pt-loaded NPs had the highest apoptosis rate (ca. 65.27% on PC3, up to ca. 63.91% on 769-P), among all the groups treated with NP1 with various cancer cells, while free *cis*-Pt could result in fewer apoptosis ratios of 8.25% for MCF-7 and 1.54% for CHO. The total apoptotic index induced by NP1 in PC3 and 769-P cell lines was 10 times higher than that of the free *cis*-Pt (6.23% and 6.17%). For NP1, the ratio became higher up to ∼1.6−2 times in MCF-7 and MDA-MB-231. The main reason is that NP1 has better cell penetration because of GLUT metabolism as we mentioned previously, which induced a larger early apoptotic index in malignant cells than that of free *cis*-Pt. NP2 also showed increased apoptosis rates for all cell lines except MCF-7. Gonzalez et al. showed that cells take up mannose into the cytoplasm through the same transporters as glucose.[59] Recent

Table 4. Comparison of Percentage of Total Apoptotic Cells with NPs and Free *cis*-Pt-Treated Cells

cell lines	*cis*-Pt	NP1	NP2	NP3
MCF-7	8.25	13.83	8.19	8.01
MDA-MB-231	7.50	14.05	18.10	16.90
PC3	6.23	65.27	14.50	9.56
769-P	6.17	63.91	27.75	12.40
CHO	1.54	46.24	14.78	6.09

DOI: 10.1021/acs.biomac.9b00528
Biomacromolecules 2019, 20, 2962−2972

evidence suggests that mannose inhibits tumor cell growth by interfering metabolism of glucose which subsequently alters the cellular response to chemotherapeutic drugs.[59] NP3 showed better apoptosis activity than *cis*-Pt alone; as upregulation of fucosylation patterns occurs in most cancer cell lines, fucose may be a ligand that actively and specifically targets these cells.[60,61]

Although all cell lines showed high apoptosis rates against NPs, factors thought to be affecting the uptake of glucosylated nanoparticles on CHO might be related to accelerated glucose metabolism of CHO cells.[62] Increased influx of glucose may explain the correlation between NPs and CHO relatively.

The rational design of well-engineered sugar-decorated nanoparticles may provide a different perspective to substrate selectivity, which may enlighten the optimization of ligands that are targeting GLUTs.[63] For maintaining high rates of glucose transport, cancer cells overexpress GLUTs in various human tumors such as breast, prostate, and renal.[64] Thus, data shown in apoptosis rates and enhanced uptake of NP1 could be associated with the overexpression of GLUT1, GLUT5, GLUT7, GLUT9, GLUT11, and GLUT12 in prostate cancer cells and GLUT1 and GLUT12 in 769-P cancer cells.[65−69] It has been shown that GLUT1 proteins are expressed in prostate cancer cell lines and protein expression levels were higher in PC3 when analyzed by western blot.[68,70−72] A number of studies have suggested a strong relationship between high GLUT-1 protein levels and renal cancer.[73−76] As can be seen, GLUTs play an important role in the oncogenesis of prostate and renal cancers. High rates of anabolic metabolism in the prostate gland results in more consumption of glucose than other tissues and is upregulated to GLUTs. For prostate cancer, even more so, glucose consumption correlates with malignancy.[77] Therefore, our study contributes to research on prostate cancer therapy by considering that malignant cells increase their glucose uptake and GLUTs expression and applying this characteristic feature may be of value for delivering drug molecules. Additionally, although chemotherapy and *cis*-Pt is not the main therapy for renal cancers,[78] our results show that glucose-transporter-directed therapy could be used in renal cancers. Higher cytotoxicity and apoptosis rates of NP1 compared with free *cis*-Pt demonstrated that the ability of glyconanopolymers for targeting prostate and renal cancer cells has strong potential.

A general outcome can be written that conjugating glycopolymer with *cis*-Pt can induce high penetration and enhance cellular uptake and apoptosis, eventually sensitizing anticancer drugs. Further research investigating the antitumor mechanism of glyconanoparticles would be worthwhile. Considering the above, these results provide important insights into the effective delivery of the *cis*-Pt-loaded glyconanoparticles, and their application to MCF-7 MDA-MB-231, PC3, and 769-P cell lines by fluorescence microscopy result in higher cytotoxicity in renal and prostate cancer cell lines.

CONCLUSIONS

Our aim was to design and develop new *cis*-Pt-loaded glyconanoparticles that can modulate the molecular process and pathways associated with tumor suppression. The *cis*-Pt-conjugated diblock glycopolymers were shown to self-assemble in aqueous solutions to form spherical nanosized assemblies with *cis*-Pt core surrounded by a glycopolymer shell, which can be utilized for intracellular detection of cancer cells. TEM revealed that approximately 100 nm nanoparticles were obtained. P(GlcMA-*b*-MAEMA), P(ManMA-*b*-MAEMA), and P(FucMA-*b*-MAEMA) formed nanoparticles with *cis*-Pt that were colloidally stable from aggregation in physiological and serum conditions as demonstrated by DLS. DLS data also showed that the hydrodynamic diameter of the NPs was increased after the *cis*-Pt conjugate, which is consistent with the TEM results. In subsequent fluorescence microscopy and flow cytometry analyses, cancer cells efficiently internalized glycopolymer-based nanoparticles. The percentage of apoptotic cells in the NP1-treated PC3 and 769-P cancer cell lines was significantly higher than those of other groups. *cis*-Pt was unable to induce high levels of apoptosis. The outstanding apoptosis performance of NP1 is attributed to the surface coating with glucose, which promotes the accumulation of NP1 within cancer cells because of the GLUT overexpression and glycolysis metabolism in PC3 and 769-P cancer cell lines. The NP1 nanoformulations are thus a promising treatment for PC3 and 769-P cancer cell lines.

Our work highlights the safety and efficiency of in vitro drug delivery system and also potentially emphasizes the importance of well-designed surface chemistry for different glyconanoparticle-based drug delivery system progresses.

We believe that such biocompatible and biomimetic glyconanoparticles conjugated with *cis*-Pt might be favorable nanocarriers for drug delivery systems and alternative nanotherapeutics affording superior anticancer efficacy as they can better target cancer cells.

ASSOCIATED CONTENT

Supporting Information

The Supporting Information is available free of charge on the ACS Publications website at DOI: 10.1021/acs.biomac.9b00528.

Characterization procedures and NMR, FT-IR, GPC, DLS, TGA ICP-MS, UV−vis, MTT assay, and apoptosis data (PDF)

AUTHOR INFORMATION

Corresponding Author

*E-mail: adag@bezmialem.edu.tr.

ORCID

Aydan Dag: 0000-0002-1552-8030

Notes

The authors declare no competing financial interest.

ACKNOWLEDGMENTS

The authors are grateful for the financial support from The Scientific & Technological Research Council of Turkey (TUBITAK) (project no. 115Z484). The Authors also thank Bezmialem Vakif University (The Scientific Research Project, 6.2015/17). The authors would also like to acknowledge Prof. Dr. Ali Durmus for his precious help in SEM images and TGA analyses.

REFERENCES

(1) Muddineti, O. S.; Ghosh, B.; Biswas, S. Current trends in using polymer coated gold nanoparticles for cancer therapy. *Int. J. Pharm.* **2015**, *484*, 252−267.

(2) Yilmaz, G.; Becer, C. R. Glyconanoparticles and their interactions with lectins. *Polym. Chem.* **2015**, *6*, 5503−5514.

DOI: 10.1021/acs.biomac.9b00528
Biomacromolecules 2019, 20, 2962−2972

(3) Babiuch, K.; Dag, A.; Zhao, J.; Lu, H.; Stenzel, M. H. Carbohydrate-Specific Uptake of Fucosylated Polymeric Micelles by Different Cancer Cell Lines. *Biomacromolecules* **2015**, *16*, 1948−1957.
(4) Tong, R.; Cheng, J. Anticancer Polymeric Nanomedicines. *Polym. Rev.* **2007**, *47*, 345−381.
(5) Figg, C. A.; Simula, A.; Gebre, K. A.; Tucker, B. S.; Haddleton, D. M.; Sumerlin, B. S. Polymerization-induced thermal self-assembly (PITSA). *Chem. Sci.* **2015**, *6*, 1230−1236.
(6) Piffoux, M.; Silva, A. K. A.; Wilhelm, C.; Gazeau, F.; Tareste, D. Modification of Extracellular Vesicles by Fusion with Liposomes for the Design of Personalized Biogenic Drug Delivery Systems. *ACS Nano* **2018**, *12*, 6830−6842.
(7) El Kazzouli, S.; Mignani, S.; Bousmina, M.; Majoral, J.-P. Dendrimer therapeutics: covalent and ionic attachments. *New J. Chem.* **2012**, *36*, 227−240.
(8) Pooja, D.; Sistla, R.; Kulhari, H. Dendrimer-drug conjugates: Synthesis strategies, stability and application in anticancer drug delivery. In *Design of Nanostructures for Theranostics Applications*; Grumezescu, A. M., Ed.; William Andrew Publishing, 2018; Chapter 7, pp 277−303.
(9) Wang, X.; Cai, X.; Hu, J.; Shao, N.; Wang, F.; Zhang, Q.; Xiao, J.; Cheng, Y. Glutathione-triggered "off-on" release of anticancer drugs from dendrimer-encapsulated gold nanoparticles. *J. Am. Chem. Soc.* **2013**, *135*, 9805−9810.
(10) Bolu, B. S.; Sanyal, R.; Sanyal, A. Drug Delivery Systems from Self-Assembly of Dendron-Polymer Conjugates (dagger). *Molecules* **2018**, *23*, 1570.
(11) An, J.; Dai, X.; Wu, Z.; Zhao, Y.; Lu, Z.; Guo, Q.; Zhang, X.; Li, C. An Acid-Triggered Degradable and Fluorescent Nanoscale Drug Delivery System with Enhanced Cytotoxicity to Cancer Cells. *Biomacromolecules* **2015**, *16*, 2444−2454.
(12) Klok, H.-A.; Lecommandoux, S. Supramolecular Materials via Block Copolymer Self-Assembly. *Adv. Mater.* **2001**, *13*, 1217−1229.
(13) Huynh, V. T.; Quek, J. Y.; de Souza, P. L.; Stenzel, M. H. Block copolymer micelles with pendant bifunctional chelator for platinum drugs: effect of spacer length on the viability of tumor cells. *Biomacromolecules* **2012**, *13*, 1010−1023.
(14) Oberoi, H.; Nukolova, N. V.; Laquer, F. C.; Poluektova, L. Y.; Alnouti, J.; Yokohira, Y.; Arnold, M.; Kabanov, A.; Cohen, A. V.; Bronich, S. M.; Huang, T. K. Cisplatin-loaded core cross-linked micelles: comparative pharmacokinetics, antitumor activity, and toxicity in mice. *Int. J. Nanomed.* **2012**, *7*, 2557−2571.
(15) San Miguel, V.; Limer, A. J.; Haddleton, D. M.; Catalina, F.; Peinado, C. Biodegradable and thermoresponsive micelles of triblock copolymers based on 2-(N,N-dimethylamino)ethyl methacrylate and ε-caprolactone for controlled drug delivery. *Eur. Polym. J.* **2008**, *44*, 3853−3863.
(16) Kawaguchi, H. Functional polymer microspheres. *Prog. Polym. Sci.* **2000**, *25*, 1171−1210.
(17) Shim, M. S.; Kwon, Y. J. Stimuli-responsive polymers and nanomaterials for gene delivery and imaging applications. *Adv. Drug Delivery Rev.* **2012**, *64*, 1046−1059.
(18) Barreto, J. A.; O'Malley, W.; Kubeil, M.; Graham, B.; Stephan, H.; Spiccia, L. Nanomaterials: applications in cancer imaging and therapy. *Adv. Mater.* **2011**, *23*, H18−H40.
(19) Spokoyny, A. M.; Kim, D.; Sumrein, A.; Mirkin, C. A. Infinite coordination polymer nano- and microparticle structures. *Chem. Soc. Rev.* **2009**, *38*, 1218−1227.
(20) Huang, J.; Bonduelle, C.; Thévenot, J.; Lecommandoux, S.; Heise, A. Biologically active polymersomes from amphiphilic glycopeptides. *J. Am. Chem. Soc.* **2012**, *134*, 119−122.
(21) Pearson, S.; Chen, G.; Stenzel, M. H. Synthesis of Glycopolymers. In *Engineered Carbohydrate-Based Materials for Biomedical Applications*; Narain, R., Ed.; John Wiley & Sons, Inc. Publishing, 2010; pp 1−118.
(22) Yilmaz, G.; Becer, C. R. Precision glycopolymers and their interactions with lectins. *Eur. Polym. J.* **2013**, *49*, 3046−3051.
(23) Vandewalle, S.; Wallyn, S.; Chattopadhyay, S.; Becer, C. R.; Du Prez, F. Thermoresponsive hyperbranched glycopolymers: Synthesis, characterization and lectin interaction studies. *Eur. Polym. J.* **2015**, *69*, 490−498.
(24) Lundquist, J. J.; Toone, E. J. The Cluster Glycoside Effect. *Chem. Rev.* **2002**, *102*, 555−578.
(25) Jamieson, E. R.; Lippard, S. J. Structure, Recognition, and Processing of Cisplatin−DNA Adducts. *Chem. Rev.* **1999**, *99*, 2467−2498.
(26) Mochida, Y.; Cabral, H.; Kataoka, K. Polymeric micelles for targeted tumor therapy of platinum anticancer drugs. *Expert Opin. Drug Delivery* **2017**, *14*, 1423−1438.
(27) Tauhardt, L.; Pretzel, D.; Bode, S.; Czaplewska, J. A.; Kempe, K.; Gottschaldt, M.; Schubert, U. S. Synthesis andin vitroactivity of platinum containing 2-oxazoline-based glycopolymers. *J. Polym. Sci., Part A: Polym. Chem.* **2014**, *52*, 2703−2714.
(28) Huynh, V. T.; de Souza, P.; Stenzel, M. H. Polymeric Micelles with Pendant Dicarboxylato Chelating Ligands Prepared via a Michael Addition forcis-Platinum Drug Delivery. *Macromolecules* **2011**, *44*, 7888−7900.
(29) Browning, R. J.; Reardon, P. J. T.; Parhizkar, M.; Pedley, R. B.; Edirisinghe, M.; Knowles, J. C.; Stride, E. Drug Delivery Strategies for Platinum-Based Chemotherapy. *ACS Nano* **2017**, *11*, 8560−8578.
(30) Yan, N. A Glimpse of Membrane Transport through Structures-Advances in the Structural Biology of the GLUT Glucose Transporters. *J. Mol. Biol.* **2017**, *429*, 2710−2725.
(31) Barron, C. C.; Bilan, P. J.; Tsakiridis, T.; Tsiani, E. Facilitative glucose transporters: Implications for cancer detection, prognosis and treatment. *Metabolism* **2016**, *65*, 124−139.
(32) Thorens, B.; Mueckler, M. Glucose transporters in the 21st Century. *Am. J. Physiol.: Endocrinol. Metab.* **2010**, *298*, E141−E145.
(33) Warburg, O. On the Origin of Cancer Cells. *Science* **1956**, *123*, 309−314.
(34) Zheng, J. Energy metabolism of cancer: Glycolysis versus oxidative phosphorylation (Review). *Oncol. Lett.* **2012**, *4*, 1151−1157.
(35) Vander Heiden, M. G.; Cantley, L. C.; Thompson, C. B. Understanding the Warburg effect: the metabolic requirements of cell proliferation. *Science* **2009**, *324*, 1029−1033.
(36) Adekola, K.; Rosen, S. T.; Shanmugam, M. Glucose transporters in cancer metabolism. *Curr. Opin. Oncol.* **2012**, *24*, 650−654.
(37) Hamanaka, R. B.; Chandel, N. S. Targeting glucose metabolism for cancer therapy. *J. Exp. Med.* **2012**, *209*, 211−215.
(38) Ganapathy-Kanniappan, S.; Geschwind, J.-F. H. Tumor glycolysis as a target for cancer therapy: progress and prospects. *Mol. Cancer* **2013**, *12*, 152.
(39) Yokoyama, M.; Okano, T.; Sakurai, Y.; Suwa, S.; Kataoka, K. Introduction of cisplatin into polymeric micelle. *J. Controlled Release* **1996**, *39*, 351−356.
(40) Ahmed, M.; Narain, R. Cell line dependent uptake and transfection efficiencies of PEI-anionic glycopolymer systems. *Biomaterials* **2013**, *34*, 4368−4376.
(41) Parry, A. L.; Clemson, N. A.; Ellis, J.; Bernhard, S. S. R.; Davis, B. G.; Cameron, N. R. Multicopy multivalent glycopolymer-stabilized gold nanoparticles as potential synthetic cancer vaccines. *J. Am. Chem. Soc.* **2013**, *135*, 9362−9365.
(42) Miura, Y.; Hoshino, Y.; Seto, H. Glycopolymer Nanobiotechnology. *Chem. Rev.* **2016**, *116*, 1673−1692.
(43) Lu, M.; Khine, Y. Y.; Chen, F.; Cao, C.; Garvey, C. J.; Lu, H.; Stenzel, M. H. Sugar Concentration and Arrangement on the Surface of Glycopolymer Micelles Affect the Interaction with Cancer Cells. *Biomacromolecules* **2019**, *20*, 273−284.
(44) Adokoh, C. K.; Quan, S.; Hitt, M.; Darkwa, J.; Kumar, P.; Narain, R. Synthesis and evaluation of glycopolymeric decorated gold nanoparticles functionalized with gold-triphenyl phosphine as anticancer agents. *Biomacromolecules* **2014**, *15*, 3802−3810.
(45) Kröger, A. P. P.; Komil, M. I.; Hamelmann, N. M.; Juan, A.; Stenzel, M. H.; Paulusse, J. M. J. Glucose Single-Chain Polymer Nanoparticles for Cellular Targeting. *ACS Macro Lett.* **2019**, *8*, 95−101.

DOI: 10.1021/acs.biomac.9b00528
Biomacromolecules 2019, 20, 2962−2972

(46) Oliveri, V.; Bentivegna, F.; Caputo, L.; Quintieri, L.; Viale, M.; Maric, I.; Lentini, G.; Vecchio, G. Positional isomers of mannose−quinoline conjugates and their copper complexes: exploring the biological activity. *New J. Chem.* **2018**, *42*, 8882−8890.
(47) Jiang, Y.; Lu, H.; Khine, Y. Y.; Dag, A.; Stenzel, M. H. Polyion complex micelle based on albumin-polymer conjugates: multifunctional oligonucleotide transfection vectors for anticancer chemotherapeutics. *Biomacromolecules* **2014**, *15*, 4195−4205.
(48) Huynh, V. T.; Chen, G.; Souza, P. d.; Stenzel, M. H. Thiol−yne and Thiol−ene "Click" Chemistry as a Tool for a Variety of Platinum Drug Delivery Carriers, from Statistical Copolymers to Crosslinked Micelles. *Biomacromolecules* **2011**, *12*, 1738−1751.
(49) Dag, A.; Lu, H.; Stenzel, M. Controlling the morphology of glyco-nanoparticles in water using block copolymer mixtures: the effect on cellular uptake. *Polym. Chem.* **2015**, *6*, 7812−7820.
(50) Schneider, C. A.; Rasband, W. S.; Eliceiri, K. W. NIH Image to ImageJ: 25 years of image analysis. *Nat. Methods* **2012**, *9*, 671−675.
(51) Khan, A.; Gillis, K.; Clor, J.; Tyagarajan, K. Simplified evaluation of apoptosis using the Muse cell analyzer. *Postep. Biochem.* **2012**, *58*, 492−496.
(52) Dag, A.; Callari, M.; Lu, H.; Stenzel, M. H. Modulating the cellular uptake of platinum drugs with glycopolymers. *Polym. Chem.* **2016**, *7*, 1031−1036.
(53) Huynh, V. T.; Binauld, S.; de Souza, P. L.; Stenzel, M. H. Acid Degradable Cross-Linked Micelles for the Delivery of Cisplatin: A Comparison with Nondegradable Cross-Linker. *Chem. Mater.* **2012**, *24*, 3197−3211.
(54) Kelland, L. The resurgence of platinum-based cancer chemotherapy. *Nat. Rev. Cancer* **2007**, *7*, 573.
(55) Mueckler, M.; Thorens, B. The SLC2 (GLUT) family of membrane transporters. *Mol. Aspects Med.* **2013**, *34*, 121−138.
(56) Zamora-Leon, S. P.; Golde, D. W.; Concha, II; Rivas, C. I.; Delgado-Lopez, F.; Baselga, J.; Nualart, F.; Vera, J. C. Expression of the fructose transporter GLUT5 in human breast cancer. *Proc. Natl. Acad. Sci. U.S.A.* **1996**, *93*, 1847−1852.
(57) Rogers, S.; Macheda, M. L.; Docherty, S. E.; Carty, M. D.; Henderson, M. A.; Soeller, W. C.; Gibbs, E. M.; James, D. E.; Best, J. D. Identification of a novel glucose transporter-like protein-GLUT-12. *Am. J. Physiol.: Endocrinol. Metab.* **2002**, *282*, E733−E738.
(58) Grover-McKay, M.; Walsh, S. A.; Seftor, E. A.; Thomas, P. A.; Hendrix, M. J. Role for glucose transporter 1 protein in human breast cancer. *Pathol. Oncol. Res.* **1998**, *4*, 115−120.
(59) Gonzalez, P. S.; O'Prey, J.; Cardaci, S.; Barthet, V. J. A.; Sakamaki, J.-i.; Beaumatin, F.; Roseweir, A.; Gay, D. M.; Mackay, G.; Malviya, G.; Kania, E.; Ritchie, S.; Baudot, A. D.; Zunino, B.; Mrowinska, A.; Nixon, C.; Ennis, D.; Hoyle, A.; Millan, D.; McNeish, I. A.; Sansom, O. J.; Edwards, J.; Ryan, K. M. Mannose impairs tumour growth and enhances chemotherapy. *Nature* **2018**, *563*, 719−723.
(60) Plattner, V. E.; Wagner, M.; Ratzinger, G.; Gabor, F.; Wirth, M. Targeted drug delivery: binding and uptake of plant lectins using human 5637 bladder cancer cells. *Eur. J. Pharm. Biopharm.* **2008**, *70*, 572−576.
(61) Yuan, X.; He, Y.; Zhou, G.; Li, X.; Feng, A.; Zheng, W. Target challenging-cancer drug delivery to gastric cancer tissues with a fucose graft epigallocatechin-3-gallate-gold particles nanocomposite approach. *J. Photochem. Photobiol., B* **2018**, *183*, 147−153.
(62) Ahn, W. S.; Antoniewicz, M. R. Metabolic flux analysis of CHO cells at growth and non-growth phases using isotopic tracers and mass spectrometry. *Metab. Eng.* **2011**, *13*, 598−609.
(63) Deng, D.; Sun, P.; Yan, C.; Ke, M.; Jiang, X.; Xiong, L.; Ren, W.; Hirata, K.; Yamamoto, M.; Fan, S.; Yan, N. Molecular basis of ligand recognition and transport by glucose transporters. *Nature* **2015**, *526*, 391.
(64) Macheda, M. L.; Rogers, S.; Best, J. D. Molecular and cellular regulation of glucose transporter (GLUT) proteins in cancer. *J. Cell. Physiol.* **2005**, *202*, 654−662.
(65) Effert, P.; Beniers, A. J.; Tamimi, Y.; Handt, S.; Jakse, G. Expression of Glucose Transporter 1 (Glut-1) in Cell Lines and Clinical Specimens from Human Prostate Adenocarcinoma. *Anticancer Res.* **2004**, *24*, 3057−3063.
(66) Reinicke, K.; Sotomayor, P.; Cisterna, P.; Delgado, C.; Nualart, F.; Godoy, A. Cellular distribution of Glut-1 and Glut-5 in benign and malignant human prostate tissue. *J. Cell. Biochem.* **2012**, *113*, 553−562.
(67) Poulose, N.; Mills, I. G.; Steele, R. E. The impact of transcription on metabolism in prostate and breast cancers. *Endocr.-Relat. Cancer* **2018**, *25*, R435−R452.
(68) Chandler, J. D.; Williams, E. D.; Slavin, J. L.; Best, J. D.; Rogers, S. Expression and localization of GLUT1 and GLUT12 in prostate carcinoma. *Cancer* **2003**, *97*, 2035−2042.
(69) Szablewski, L. Expression of glucose transporters in cancers. *Biochim. Biophys. Acta* **2013**, *1835*, 164−169.
(70) Carvalho, K. C.; Cunha, I. W.; Rocha, R. M.; Ayala, F. R.; Cajaíba, M. M.; Begnami, M. D.; Vilela, R. S.; Paiva, G. R.; Andrade, R. G.; Soares, F. A. GLUT1 expression in malignant tumors and its use as an immunodiagnostic marker. *Clinics* **2011**, *66*, 965−972.
(71) Xiao, H.; Wang, J.; Yan, W.; Cui, Y.; Chen, Z.; Gao, X.; Wen, X.; Chen, J. GLUT1 regulates cell glycolysis and proliferation in prostate cancer. *Prostate* **2018**, *78*, 86−94.
(72) Gonzalez-Menendez, P.; Hevia, D.; Rodriguez-Garcia, A.; Mayo, J. C.; Sainz, R. M. Regulation of GLUT transporters by flavonoids in androgen-sensitive and -insensitive prostate cancer cells. *Endocrinology* **2014**, *155*, 3238−3250.
(73) Singer, K.; Kastenberger, M.; Gottfried, E.; Hammerschmied, C. G.; Büttner, M.; Aigner, M.; Seliger, B.; Walter, B.; Schlösser, H.; Hartmann, A.; Andreesen, R.; Mackensen, A.; Kreutz, M. Warburg phenotype in renal cell carcinoma: high expression of glucose-transporter 1 (GLUT-1) correlates with low CD8(+) T-cell infiltration in the tumor. *Int. J. Cancer* **2011**, *128*, 2085−2095.
(74) Brodaczewska, K. K.; Szczylik, C.; Fiedorowicz, M.; Porta, C.; Czarnecka, A. M. Choosing the right cell line for renal cell cancer research. *Mol. Cancer* **2016**, *15*, 83.
(75) Page, T.; Hodgkinson, A. D.; Ollerenshaw, M.; Hammonds, J. C.; Demaine, A. G. Glucose transporter polymorphisms are associated with clear-cell renal carcinoma. *Cancer Genet. Cytogenet.* **2005**, *163*, 151−155.
(76) Chan, D. A.; Sutphin, P. D.; Nguyen, P.; Turcotte, S.; Lai, E. W.; Banh, A.; Reynolds, G. E.; Chi, J.-T.; Wu, J.; Solow-Cordero, D. E.; Bonnet, M.; Flanagan, J. U.; Bouley, D. M.; Graves, E. E.; Denny, W. A.; Hay, M. P.; Giaccia, A. J. Targeting GLUT1 and the Warburg effect in renal cell carcinoma by chemical synthetic lethality. *Sci. Transl. Med.* **2011**, *3*, 94ra70.
(77) Zhang, Y.; Fang, L.; Zang, Y.; Ren, J.; Xu, Z. CIP2A Promotes Proliferation, Invasion and Chemoresistance to Cisplatin in Renal Cell Carcinoma. *J. Cancer* **2018**, *9*, 4029−4038.
(78) Zhang, Y.; Fang, L.; Zang, Y.; Ren, J.; Xu, Z. CIP2A Promotes Proliferation, Invasion and Chemoresistance to Cisplatin in Renal Cell Carcinoma. *J. Cancer* **2018**, *9*, 4029−4038.

DOI: 10.1021/acs.biomac.9b00528
Biomacromolecules 2019, 20, 2962−2972